

Parallel and heralded multiqubit entanglement generation for quantum networks

Hui Zhou (周辉),¹ Tao Li (李涛) ^{1,3,*} and Keyu Xia (夏可宇) ^{2,3}

¹*MIIT Key Laboratory of Semiconductor Microstructure and School of Science, Nanjing University of Science and Technology, Nanjing 210094, China*

²*College of Engineering and Applied Sciences and School of Physics, Nanjing University, Nanjing 210023, China*

³*National Laboratory of Solid State Microstructures, Collaborative Innovation Center of Advanced Microstructures, Nanjing University, Nanjing 210023, China*



(Received 3 November 2022; revised 8 February 2023; accepted 13 February 2023; published 21 February 2023)

Quantum networks involving multiqubit entanglement allow exciting applications in quantum communication, quantum sensing, and distributed quantum computation. The efficiency of nonlocal entanglement generation through optical channels drops exponentially with the distance between network nodes. We present a parallel and heralded protocol for generating distributed multiqubit entanglement across multiple nodes. This is achieved by using a high-dimensional single photon that works as a common-data bus connecting all stationary qubits (i.e., silicon-vacancy electron spins), each of which is coupled to a single-sided optical cavity. Parallel multiqubit entangled states are heralded by the detection of the single photon after it interacts with each stationary qubit and passes through each photonic modulation circuit. This parallel protocol can significantly improve the efficiency of distributed entanglement generation and provides a viable route towards distributed multinode quantum networks.

DOI: [10.1103/PhysRevA.107.022428](https://doi.org/10.1103/PhysRevA.107.022428)

I. INTRODUCTION

Quantum entanglement is probably the most important aspect of quantum theory. It has attracted a great deal of attention not only for its distinctly nonclassical properties but also for its numerous incomparable applications in quantum information science [1,2]. Quantum entanglement between quantum network nodes enables quantum secure communication [3–7], distributed quantum sensing [8–10], and distributed quantum computation [11–14]. To entangle two remote nodes, a single photon entangled with a stationary qubit at one node [15] either interferes with a similar photon entangled with a stationary qubit at the other node [16–20] or directly interacts with this stationary qubit [21–26]. However, the photon transmission rate degrades exponentially with the distance between two nodes, which limits the entanglement generation rate and then the performance of a practical quantum network [27–31]. Recently, quantum multiplexing with each photon carrying two qubits has been proposed to enhance the entanglement generation rate between two distant nodes [32] and to reduce the resources required for faithful quantum state transfer with error-correction codes [33].

Greenberger-Horne-Zeilinger (GHZ) states, entangling more than two qubits, constitute a valuable resource for implementing quantum information tasks [34]. They have been used to perform the strongest test of local realism [35] and to implement quantum networking technologies ranging from multiparty quantum communication [36–39] to quantum metrology [40] and quantum error correction [41]. In prin-

ciple, distributed multiqubit GHZ states can be generated by locally preparing them [42–45] and distributing each qubit, i.e., photon or flying qubit, to one distant node to interact with a stationary qubit [46,47]. However, this approach requires that all photons arrive at their destination nodes [48]. Its generation rate degrades exponentially and equals that achieved by subsequently interacting a photon with each stationary qubit. Alternatively, GHZ states among distant nodes can be generated by entanglement swapping [49–52], given a prior distribution of entangled pairs [27–29]. While distributed two-qubit entanglements between two quantum network nodes have been demonstrated with various physical implementations [53], further progress towards distributed multiqubit entanglements [54–56] has been hampered by the finite photon transmission rate and inefficient stationary qubits.

Here we present a parallel and heralded protocol for generating distributed entanglement among multiple stationary qubits located in distant network nodes. We break the rapidly increasing transmission-loss limit [57–59] using temporal multiplexing and successfully entangle multiple sets of stationary qubits with the transmission of a single photon in a heralded fashion. A stationary qubit coupled to an optical microcavity allows for an effective interface between single photons and individual spins via state-dependent reflection when photons impinge on the microcavity [60–63]. A single photon, acting as a high-capacity common-data bus [64], carries one polarization qubit and one time-bin qudit. It can entangle MN stationary qubits, i.e., electron spins, by subsequently interacting with them, leading to the generation of MN -spin GHZ states among N distant network nodes, each of which contains M stationary qubits. The entanglement generation rate of distributed GHZ states, in principle, can be

*tao.li@njust.edu.cn

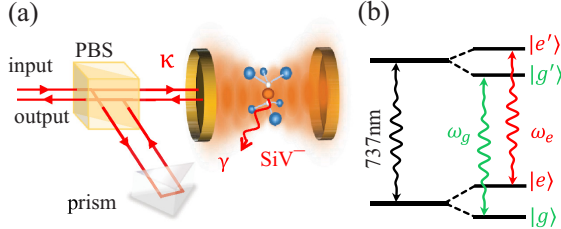


FIG. 1. (a) Schematic of the controlled-polarization flip unit based on a SiV^- in diamond coupled to a single-sided microcavity. (b) Level structure of a SiV^- and its optical transitions.

increased by a factor inversely proportional to the M th power of the transmission rate. Therefore, our parallel protocol can provide a promising avenue for various distributed multinode quantum networks.

The paper is organized as follows. A quantum interface between a single photon and a SiV^- electron spin is introduced briefly in Sec. II to constitute a fundamental building block. In Sec. III a parallel and heralded protocol for generating MN -spin GHZ states with the transmission of a single photon is presented. Subsequently, the performance of multiqubit entanglement generation is discussed in Sec. IV. We provide a brief discussion in Sec. V and a summary in Sec. VI. Finally, the Appendix presents a simple example of our protocol for generating two three-spin GHZ states across three distant nodes.

II. FUNDAMENTAL BUILDING BLOCK

A fundamental building block of our protocol is an efficient interface between a single photon and an individual spin, which can constitute a controlled-polarization flip (CPF) unit. The CPF unit, in principle, entangles the spin and the photonic polarization qubits and thus enables a polarized photon in time-bin qudit states to serially entangle each spin qubit to create $M \geq 2$ GHZ states across $N \geq 3$ distant network nodes. The total distance the photon needs to travel in our parallel scheme for generating M GHZ states is identical to that in other schemes for generating one GHZ state, speeding up the efficiency of multiqubit GHZ-state generation for large-scale quantum networks.

We consider a specific CPF unit outlined in Fig. 1, which is implemented by a negatively charged silicon vacancy center (SiV^-) in diamond coupled to a single-sided microcavity resonance near 737 nm. A SiV^- center consists of complexes made up of two carbon vacancies between which is a silicon atom [61–63], shown in Fig. 1(a). The resulting D_{3d} inversion symmetry of a SiV^- center about the Si atom results in a vanishing electron dipole moment of the ground and excited states [61]. The SiV^- centers are therefore more resilient to electrical noise typically present in nanophotonic structures and have better optical properties than nitrogen-vacancy color centers at low temperatures (below 500 mK) [62]. The energy levels of a SiV^- center under moderate strain can be simplified to two electron-spin sublevels of the lowest orbital branch in the ground state, i.e., $|g\rangle = |\downarrow\rangle$ and $|e\rangle = |\uparrow\rangle$, and two electron-spin sublevels of the lower orbital branch in the excited state, i.e., $|g'\rangle = |\downarrow'\rangle$ and $|e'\rangle = |\uparrow'\rangle$ [62], after

removing irrelevant levels with large detunings, shown in Fig. 1(b). These states are connected by two spin-conserving optical transitions with horizontal polarization, i.e., $|H\rangle$, and frequencies ω_g and $\omega_e = \omega_g + \Delta$, when an external magnetic field is applied along the SiV^- symmetry axis. Meanwhile, the cross transitions with spin flipping are dipole forbidden and can be neglected [62].

Suppose an H -polarized photon with frequency ω impinges on the input port of a SiV^- -cavity system; its frequency is near resonance with the cavity mode ($\omega \simeq \omega_c$) and the dipole transition $|g\rangle \rightarrow |g'\rangle$ but far detuned from the dipole transition $|e\rangle \rightarrow |e'\rangle$. Then the scattering will be significantly different when the SiV^- is initialized to states $|g\rangle$ and $|e\rangle$ and couples strongly with the cavity. The dynamic equations of motion for the cavity mode \hat{a} and the dipole operator $\hat{\sigma}_-$ as well as the input-output relation can be described by [21,65]

$$\begin{aligned} \frac{d\hat{a}}{dt} &= -\left(i(\omega_c - \omega) + \frac{\kappa}{2}\right)\hat{a} - g\hat{\sigma}_- - \sqrt{\kappa}\hat{a}_{\text{in}} + \hat{N}, \\ \frac{d\hat{\sigma}_-}{dt} &= -\left(i(\omega_s - \omega) + \frac{\gamma}{2}\right)\hat{\sigma}_- - g\hat{\sigma}_z\hat{a} + \hat{N}', \\ \hat{a}_{\text{out}} &= \hat{a}_{\text{in}} + \sqrt{\kappa}\hat{a}, \end{aligned} \quad (1)$$

where ω_s (ω_c) is the dipole-transition (cavity-mode) frequency, g is the coupling rate between the SiV^- and the cavity, γ is the decay rate of the excited state, κ is the cavity decay rate, coupling to the input and output modes, and \hat{a}_{in} (\hat{a}_{out}) is the input (output) mode. The operators \hat{N} and \hat{N}' are used to preserve the desired commutation relations and they represent noises originating from the cavity leakage and dipole decay, respectively.

The reflection coefficient in the weak excitation limit with $\langle \hat{\sigma}_z \rangle \simeq -1$ can be described by [65]

$$r_s(\omega) = 1 - \frac{2(i\Delta_s + 1)}{(i\Delta_s + 1)(i\Delta_c + 1) + C}, \quad (2)$$

where $C = 4g^2/\kappa\gamma$ is the cooperativity, $\Delta_s = 2(\omega_s - \omega)/\gamma$ with subscript $s = g, e$, and $\Delta_c = 2(\omega_c - \omega)/\kappa$ are effective detunings of the dipole and the cavity mode from the input field frequency, respectively. For $\Delta_c = \Delta_g = 0$ and $\Delta_e \gg C \gg 1$, the reflection coefficient equals $r_g = 1$ ($r_e = -1$) for a SiV^- in state $|g\rangle$ ($|e\rangle$) and an input photon with horizontal polarization $|H\rangle$.

This state-dependent reflection can be used to constitute a CPF unit using a polarized photon as the target and a SiV^- as the control, shown in Fig. 1(a). The CPF unit consists of a cavity- SiV^- system, a prism that reflects all photonic modes, and a polarizing beam splitter (PBS) that reflects V -polarized photons and transmits those of horizontal polarization $|H\rangle$. Suppose an arbitrary polarized photon is in state $|\psi_p\rangle = \alpha|D\rangle + \beta|A\rangle$, where $|\alpha|^2 + |\beta|^2 = 1$, $|D\rangle = (|V\rangle + |H\rangle)/\sqrt{2}$, and $|A\rangle = (|V\rangle - |H\rangle)/\sqrt{2}$, and the SiV^- is in state $|\psi_s\rangle = (|g\rangle + |e\rangle)/\sqrt{2}$. The CPF unit evolves the photon and SiV^- electron spin into

$$|\psi_c\rangle = \frac{1}{\sqrt{2}}(|g\rangle|\psi_p\rangle + |e\rangle|\bar{\psi}_p\rangle), \quad (3)$$

where the polarization-flip state is represented by $|\bar{\psi}_p\rangle = \alpha|A\rangle + \beta|D\rangle$. This CPF unit is referred to as a SiV^-

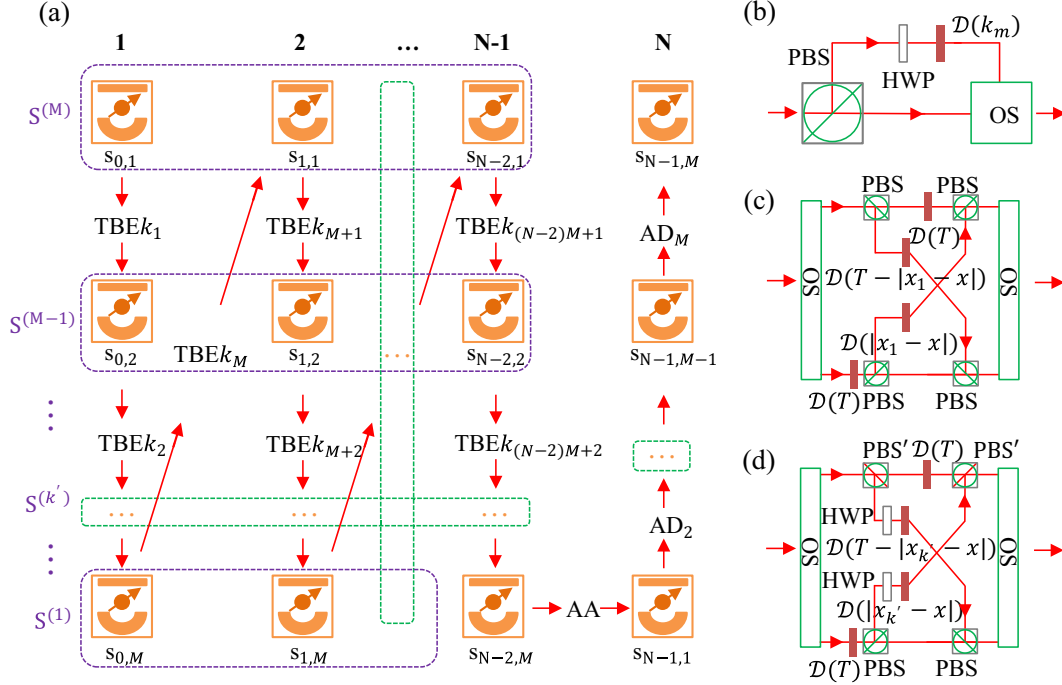


FIG. 2. Schematics of generating $M N$ -spin GHZ states across N nodes using a single photon. (a) Step-by-step protocol for generating $M N$ -spin GHZ states. (b) Time-bin encoding $TBEk_m$. (c) Swapping unit AA that exchanges two A-polarized time-bin components. (d) Swapping unit $AD_{k'}$ that exchanges two time-bin components with orthogonal polarizations. Here PBS (PBS') represents a polarizing beam splitter that reflects A-polarized (D -polarized) photons and transmits D -polarized (A-polarized) ones, HWP is a half waveplate that flips the polarization of photons, $\mathcal{D}(\ast)$ introduces a time delay that is determined by the value given in the parentheses with its maximum $T = 2^K$, and OS is an optical switch that directs two spatial modes of a photon with different time bins into one spatial mode and vice versa.

electron spin below and constitutes a fundamental building block for parallel and heralded multiqubit entanglement generation among multiple nodes for distributed quantum networks. We emphasize that our protocol can be used for distributed quantum networks involving other CPF units that are implemented by natural atoms, quantum dots, or other color centers coupled to optical cavities or waveguides [15–26].

III. PROTOCOL FOR GENERATING $M N$ -SPIN GHZ STATES WITH A SINGLE PHOTON

The scheme for generating $M N$ -spin GHZ states across N nodes, shown in Fig. 2, requires CPFs and time-bin encoding (TBE) as well as photonic swapping units, i.e., AA and $AD_{k'}$ swap two time bins with the same polarization, i.e., $|A_x\rangle$ and $|A_{x_1}\rangle$, and that with orthogonal polarizations, i.e., $|A_x\rangle$ and $|D_{x_k'}\rangle$, respectively. An input photon P with D polarization is scattered by a CPF followed by a TBE, which doubles the time bins of photon P and evolves all time bins to have D polarization, shown in Fig. 2(b). For example, the half waveplate (HWP) transfers A-polarized time-bin modes in the upper path of $TBEk_m$ to D -polarized ones and the optical delay $\mathcal{D}(k_m)$ introduces a time delay of $k_m T_\Delta$ for time-bin modes passing through it, where

$$k_m = 2^{K-m}, \quad (4)$$

with $K = (N-1)M-1$ for $m = 1, 2, \dots, K$. Subsequently, time-bin modes in both the upper and lower paths of $TBEk_m$ are D polarized and are combined into the same spatial mode

by an optical switch (OS). Note that the time interval T_Δ between two neighboring time bins should be larger than both the cavity lifetime $1/\kappa$ and the dipole lifetime $1/\Gamma$ with a cavity-enhanced dipole decay rate $\Gamma = (1+C)\gamma$. After photon P is scattered by the CPF containing the SiV^- electron spin $s_{N-2,M}$ in node $N-1$, the photon is encoded by a 2^K -dimensional time-bin mode and a two-dimensional polarization mode and maximally entangles with the $(N-1)M$ SiV^- electron spins, shown in Eq. (9). This hybrid entanglement can be converted into $M N$ -spin GHZ states by actively controlling the photon states with photonic swapping units, i.e., AA and $AD_{k'}$, before the photon impinges on each CPF in node N .

A. Hybrid entanglement of a high-dimensional single photon and $(N-1)M$ electron spins

Suppose all SiV^- electron spins, shown in Fig. 2(a), are initialized in the superposition state $|\psi_{s_{l,j}}\rangle = (|g_{s_{l,j}}\rangle + |e_{s_{l,j}}\rangle)/\sqrt{2}$ for $s_{l,j} = lM + j$, $l = 0, 1, \dots, N-1$, and $j = 1, 2, \dots, M$, and a resonant photon P with D polarization is directed to interact with $s_{0,1}$ in node 1. The photon then passes through $TBEk_1$, shown in Fig. 2(b), and converts its component $|A_0\rangle$ into $|D_{k_1}\rangle$. The state of photon P and spin $s_{0,1}$ evolves into

$$|\Phi_1\rangle = \frac{1}{\sqrt{2}}(|g_1\rangle|D_0\rangle + |e_1\rangle|D_{k_1}\rangle), \quad (5)$$

which is an entangled state of the photonic time-bin mode and electron spin $s_{0,1}$. The photon subsequently interacts with each CPF and is rearranged by a TBE. After the photon is output by TBE k_m for $m \in \{2, 3, \dots, K\}$, the state of photon P and m electron spins evolves into a hybrid entangled state

$$|\Phi_m\rangle = \frac{1}{\sqrt{2^m}} \sum_{t=0}^{2^m-1} \bigotimes_{i=1}^m \hat{\delta}_{1j_i^{(t)}} |g_1, \dots, g_m\rangle |D_{t_m}\rangle, \quad (6)$$

where t is a parameter in the decimal format, which can be translated into an m -bit binary as $j_1^{(t)} j_2^{(t)} \dots j_m^{(t)} \in \{0, 1\}$ with $t = \sum_{i=1}^m 2^{m-i} j_i^{(t)}$, and the subscript $t_m = t k_m T_\Delta$ represents the time delay. The state of the i th electron spin is $|g\rangle$ ($|e\rangle$) for $j_i^{(t)} = 0$ ($j_i^{(t)} = 1$) and the operator $\hat{\delta}_{1j_i^{(t)}}$ is

$$\hat{\delta}_{1j_i^{(t)}} = \begin{cases} \hat{\sigma}_i^X, & j_i^{(t)} = 1 \\ \hat{I}_i, & j_i^{(t)} = 0, \end{cases} \quad (7)$$

where $\hat{I}_i = |g\rangle_i \langle g| + |e\rangle_i \langle e|$ is the identity and $\hat{\sigma}_i^X = |g\rangle_i \langle e| + |e\rangle_i \langle g|$ is the spin-flip operator of the i th electron spin.

For simplicity, it is convenient to divide K electron spins into M parts $S^{(1)}, \dots, S^{(k')}, \dots, S^{(M)}$, shown in Fig. 2(a). The state of $S^{(k')}$ with all electron spins in state $|g\rangle$ and $k' = M - k + 1$ for $k = 1, 2, \dots, M$ can be described as

$$|G_{S^{(k')}}\rangle = \begin{cases} |g_{s_{0,M}} g_{s_{1,M}} \dots g_{s_{N-3,M}}\rangle, & k' = 1 \\ |g_{s_{0,k}} g_{s_{1,k}} \dots g_{s_{N-2,k}}\rangle, & k' = 2, 3, \dots, M. \end{cases} \quad (8)$$

Afterward photon P interacts with the $(K+1)$ th electron spin $s_{N-2,M}$ and its state in combination with that of $K+1$ electron spins evolves into

$$|\Phi_{K+1}\rangle = \frac{1}{\sqrt{2^{K+1}}} \sum_{x=0}^{2^K-1} |G_{S^{(1)}}\rangle_x |G_{S^{(2)}}\rangle_x \dots |G_{S^{(M)}}\rangle_x \otimes (|g_{N-2,M}\rangle |D_x\rangle + |e_{N-2,M}\rangle |A_x\rangle), \quad (9)$$

where a decimal parameter x can be translated into a K -bit binary as $j_1 j_2 \dots j_m \dots j_K$ with $x = \sum_{m=1}^K j_m k_m$ and $j_m \in \{0, 1\}$; $|G_{S^{(k')}}\rangle_x$ represents the state of $S^{(k')}$ when photon P is in the time-bin mode x : $|G_{S^{(1)}}\rangle_x = \bigotimes_{m'=0}^{N-3} \hat{\delta}_{1j_{m'}} |G_{S^{(1)}}\rangle$ and $|G_{S^{(k')}}\rangle_x = \bigotimes_{m'=0}^{N-2} \hat{\delta}_{1j_{m'}} |G_{S^{(k')}}\rangle$ for $k' = 2, 3, \dots, M$, where $m' = (m-k)/M$ is the integer value function that rounds the number $(m-k)/M$ down to the nearest integer and $\hat{\delta}_{1j_{m'}}$ is defined by Eq. (7). Furthermore, the state of electron spin $s_{N-2,M}$ is exclusively determined by the polarization of photon P , in a manner similar to that described by Eq. (5). Therefore, the state $|\Phi_{K+1}\rangle$ is a hybrid entangled state between photon P and $K+1$ electron spins, in which the time-bin state of photon P is determined by the first K electron spins, while the polarization of photon P is determined by the state of the $(K+1)$ th electron spin.

B. Heralded generation of M N -spin GHZ states

To project electron spin $s_{N-1,k'}$ ($k' = 1, \dots, M$) in node N and spins $s_{n-1,k}$ ($k = M - k' + 1$) in nodes $n = 1, 2, \dots, N - 1$ into a GHZ state, some photonic swapping units are properly applied on photon P before it interacts with electron spin $s_{N-1,k'}$. In general, the photonic time-bin mode entangles with the first K spins. For any time-bin mode x , the states of

$|G_{S^{(1)}}\rangle \dots |G_{S^{(M)}}\rangle$ are determined by the K -bit binary string $j_1 j_2 \dots j_m \dots j_K$, as shown in Eq. (9). There is a corresponding spin state that is determined by x_1 , which can be translated into a K -bit binary as $j_1^{(1)} j_2^{(1)} \dots j_m^{(1)} \dots j_K^{(1)}$ with $j_m^{(1)} = \bar{j}_m$ for $m = M, 2M, \dots, (N-2)M$ and $j_m^{(1)} = j_m$ for other values of m . The swapping unit AA consisting of OSs, optical delays $\mathcal{D}(\ast)$, and PBSs, as shown in Fig. 2(c), exchanges the photon time-bin states x with x_1 in the A -polarization mode and then evolves the state $|\Phi_{K+1}\rangle$ into

$$|\Phi'_{K+1}\rangle = \frac{1}{\sqrt{2^{K+1}}} \sum_{x=0}^{2^K-1} |G_{S^{(2)}}\rangle_x \dots |G_{S^{(M)}}\rangle_x \otimes (|G_{S^{(1)}}\rangle_x |g_{N-2,M}\rangle |D_x\rangle + |\bar{G}_{S^{(1)}}\rangle_x |e_{N-2,M}\rangle |A_x\rangle), \quad (10)$$

where the state $|\bar{G}_{S^{(1)}}\rangle_x = |G_{S^{(1)}}\rangle_{x_1} = \bigotimes_{l=0}^{N-3} \hat{\sigma}_{s_{l,M}}^X |G_{S^{(1)}}\rangle_x$ represents the bit-flip state of all electron spins of $S^{(1)}$ when the photon is in time-bin mode x .

The photon P then interacts with spin $s_{N-1,1}$ and its state in combination with $K+2$ spins can be described as

$$|\Phi_{K+2}\rangle = \frac{1}{\sqrt{2^{K+2}}} \sum_{x=0}^{2^K-1} |G_{S^{(2)}}\rangle_x \dots |G_{S^{(M)}}\rangle_x \otimes [(|G_{S^{(1)}}\rangle_x |g_{N-2,M} g_{N-1,1}\rangle + |\bar{G}_{S^{(1)}}\rangle_x |e_{N-2,M} e_{N-1,1}\rangle) |D_x\rangle + (|G_{S^{(1)}}\rangle_x |g_{N-2,M} e_{N-1,1}\rangle + |\bar{G}_{S^{(1)}}\rangle_x |e_{N-2,M} g_{N-1,1}\rangle) |A_x\rangle], \quad (11)$$

which explicitly shows the entanglement of N spins ($S^{(1)}$ and $s_{N-2,M} s_{N-1,1}$). In practice, the state $|\Phi_{K+2}\rangle$ can be projected into an N -spin GHZ state if the photon P is measured in the basis $\{|D\rangle, |A\rangle\}$ with time-resolved detectors, since the states $|G_{S^{(1)}}\rangle_x$ of the first $N-2$ spins are orthogonal for any two time bins distinguished by different subscripts x . Furthermore, this state can be modified by a swapping unit to correlate the polarization states of photon P with those of spins $S^{(2)}$, whereas states of other spins are separated from those of spins $S^{(2)}$ and the photon's polarization. The modified state thus has a form similar to $|\Phi'_{K+1}\rangle$ and can entangle spins $S^{(2)}$ and $s_{N-1,2}$ after the photon interacts with spin $s_{N-1,2}$.

The swapping unit AD_2 completing such a modification, shown in Fig. 2(d), can be constructed by OSs, $\mathcal{D}(\ast)$, PBSs and PBS's and then exchanges photon components $|A_x\rangle$ and $|D_{x_2}\rangle$ ($|A_{x_2}\rangle$ and $|D_x\rangle$) for $x < x_2$ ($x_2 < x$). Here x_2 is determined by a K -bit binary string $j_1^{(2)} j_2^{(2)} \dots j_m^{(2)} \dots j_K^{(2)}$ with $j_m^{(2)} = \bar{j}_m$ for $m = M-1, 2M-1, \dots, (N-1)M-1$ and $j_m^{(2)} = j_m$ for other values of m . The state $|\Phi_{K+2}\rangle$ is evolved into

$$|\Phi'_{K+2}\rangle = \frac{1}{\sqrt{2^{K+1}}} \sum_{x=0}^{2^K-1} |G_{S^{(3)}}\rangle_x \dots |G_{S^{(M)}}\rangle_x |\varphi_1\rangle_x \otimes (|G'_{S^{(2)}}\rangle |D_x\rangle + |\bar{G}'_{S^{(2)}}\rangle |A_x\rangle), \quad (12)$$

where $|\varphi_1\rangle_x$ represents an N -spin GHZ state and can be described as

$$|\varphi_1\rangle_x = \frac{1}{\sqrt{2}} (|G_{S^{(1)}}\rangle_x |G_{1,2}\rangle + |\bar{G}_{S^{(1)}}\rangle_x |\bar{G}_{1,2}\rangle), \quad (13)$$

with

$$|G_{1,2}\rangle = \begin{cases} |g_{N-2,M}g_{N-1,1}\rangle, & x < x_2 \\ |g_{N-2,M}e_{N-1,1}\rangle, & x > x_2, \end{cases} \quad (14)$$

and a general state $|G'_{S^{(k')}}\rangle$ of electron spins $S^{(k')}$ can be described as

$$|G'_{S^{(k')}}\rangle = \begin{cases} |G_{S^{(k')}}\rangle_x, & x < x_{k'} \\ |G_{S^{(k')}}\rangle_{x_{k'}}, & x > x_{k'} \end{cases} \quad (15)$$

for $|G_{S^{(k')}}\rangle_{x_{k'}} = \bigotimes_{l=0}^{N-2} \hat{\sigma}_{s_{l,k'}}^X |G_{S^{(k')}}\rangle_x$, $k' = 2, 3, \dots, M$.

The photon P then interacts with spin $s_{N-1,2}$ and the combined state of photon P and $K+3$ electron spins evolves into

$$\begin{aligned} |\Phi_{K+3}\rangle &= \frac{1}{\sqrt{2^{K+2}}} \sum_{x=0}^{2^K-1} |G_{S^{(3)}}\rangle_x \cdots |G_{S^{(M)}}\rangle_x |\varphi_1\rangle_x \\ &\otimes [(|G'_{S^{(2)}}\rangle |g_{N-1,2}\rangle \\ &+ |\tilde{G}'_{S^{(2)}}\rangle |e_{N-1,2}\rangle) |D_x\rangle \\ &+ (|G'_{S^{(2)}}\rangle |e_{N-1,2}\rangle \\ &+ |\tilde{G}'_{S^{(2)}}\rangle |g_{N-1,2}\rangle) |A_x\rangle]. \end{aligned} \quad (16)$$

Here spins $S^{(1)}$ and $s_{N-2,M}s_{N-1,1}$ and spins $S^{(2)}$ and $s_{N-1,2}$ are simultaneously in GHZ states, whereas all other spins are separable from them.

This entangling operation can be cascaded to project more electron spins into GHZ states by modifying the photon states with a proper swapping unit $AD_{k'}$ ($k' = 2, 3, \dots, M$) before interacting photon P with the corresponding electron spin $s_{N-1,k'}$. Here the $AD_{k'}$ exchanges photon components $|A_x\rangle$ and $|D_{x_{k'}}\rangle$ for $x < x_{k'}$ and $|A_{x_{k'}}\rangle$ and $|D_x\rangle$ for $x_{k'} < x$. The subscript $x_{k'}$ is determined by a K -bit binary string $j_1^{(k')}j_2^{(k')} \cdots j_m^{(k')} \cdots j_K^{(k')}$ with $j_m^{(k')} = \bar{j}_m$ for $m = k, M+k, \dots, (N-2)M+k$ and $j_m^{(k')} = j_m$ for other values of m . Therefore, after photon P interacts with $s_{N-1,M}$, the state of MN electron spins and photon P evolves into

$$\begin{aligned} |\Phi_{K+M+1}\rangle &= \frac{1}{\sqrt{2^{K+2}}} \sum_{x=0}^{2^K-1} |\varphi_1\rangle_x \bigotimes_{k'=2}^{M-1} |\varphi_{k'}\rangle_x \\ &\otimes [(|G'_{S^{(M)}}\rangle |g_{N-1,M}\rangle \\ &+ |\tilde{G}'_{S^{(M)}}\rangle |e_{N-1,M}\rangle) |D_x\rangle \\ &+ (|G'_{S^{(M)}}\rangle |e_{N-1,M}\rangle \\ &+ |\tilde{G}'_{S^{(M)}}\rangle |g_{N-1,M}\rangle) |A_x\rangle], \end{aligned} \quad (17)$$

where the k' th N -spin GHZ state for $k' = 2, \dots, M-1$ is

$$|\varphi_{k'}\rangle_x = \frac{1}{\sqrt{2}} (|G'_{S^{(k')}}\rangle |g_{N-1,k'}\rangle + |\tilde{G}'_{S^{(k')}}\rangle |e_{N-1,k'}\rangle), \quad (18)$$

which is determined by the photon's time bin x and its value relative to $x_{k'}$, while the M th N -spin GHZ state is determined by the photon's time bin and polarization state, which can be determined by time-resolved detectors. A simple example, i.e., $N = 3$ and $M = 2$, for the generation of two three-spin GHZ states with the transmission of a single photon is presented in the Appendix.

IV. PERFORMANCE OF OUR PARALLEL PROTOCOL FOR GENERATING MULTIQUBIT ENTANGLEMENT ACROSS MULTIPLE NODES

So far, we have assumed indistinguishable CPFs with identical optical transitions and a perfect model where the interface between single photons and individual spins is deterministic with opposite phases for an input H -polarization photon with frequency ω and a SiV^- electron spin in states $|g\rangle$ and $|e\rangle$. However, SiV^- centers have different optical transition detunings due to variations of local strain and external fields. It is therefore necessary to actively compensate these detunings by tuning the strain and external fields [66–68]. Meanwhile, there are always some imperfections that introduce a deviation from this ideal interface, such as a finite detuning Δ_e and a finite cooperativity C due to a limited coupling g between an electron spin and an optical nanocavity, and that lead to a realistic (nonideal) scattering coefficient $r_s(\omega)$ given in Eq. (2).

Fortunately, the influence of this nonideal scattering on the fidelity of multiqubit entanglement generation can be passively suppressed in a heralded way, reducing the efficiency of entanglement generation; a semi-ideal interface with an identical reflection probability and opposite phases can be achieved for scattering processes with an electron spin in states $|g\rangle$ and $|e\rangle$. For instance, the reflection coefficient is $r_g = -r_e = 0.98$ for an input H -polarization photon with $C = 100$, $\Delta_c = 1$, and $\Delta_e = 100$. Taking experimental accessible parameters $(g, \kappa, \gamma) = 2\pi \times (8.4, 28.2, 0.1)$ GHz [63], the cooperativity $C = 100$ can be achieved for a system consisting of a SiV^- coupled to a nanocavity. Meanwhile, the large optical splitting of these two optical transitions ($\Delta_c - \Delta_e = 99$) can be achieved at magnetic field $B \sim 0.5$ T and moderate strain ($\sim 10^{-7}$ strain) under which the difference of Landé g factors in the excited and ground states can be $\delta g = 0.06$ and the orbital splitting of ground state is $\Delta_{gs} \sim 140$ GHz [62].

Our parallel protocol generates M N -qubit GHZ states among N nodes by using a high-dimensional single photon as a common-data bus connecting MN electron spins. The single photon is effectively scattered once by each CPF and it involves MN scattering processes in our protocol. The efficiency of our protocol is mainly limited by the channel transmission loss and the scattering loss, when the time-bin encoding and swapping units, consisting of linear optical elements and OSs, are ideal and introduce negligible errors.

For simplicity, we assume the distance between two adjacent nodes is L and the total optical channel length is $(N-1)L$ for an N -node network. The efficiency of our parallel protocol for generating M N -qubit GHZ states among N nodes is

$$\eta_{N,M} = \eta_0^{NM} \eta_d \exp[-\alpha(N-1)L], \quad (19)$$

where $\eta_0 = |r_0|^2 = 0.96$ is the probability that the single photon is channeled to an optical circuit after scattering, $\eta_d \geq 0.96$ is the detection efficiency of single-photon detectors, and α is the attenuation coefficient of optical channels with $\alpha \simeq \frac{1}{22} \text{ km}^{-1}$ [27]. However, for protocols that entangle each N spins using one photon as a common-data bus, they require the transmission and detection of M photons for generating M N -qubit GHZ states among N nodes. Therefore, the

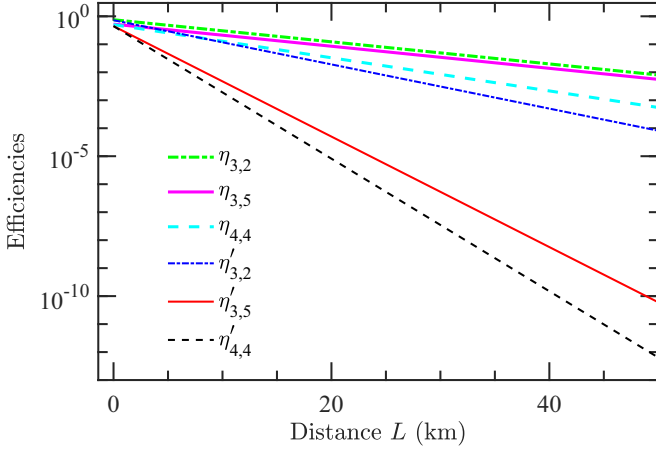


FIG. 3. Efficiencies of entanglement generation for M N -spin GHZ states. The distance L between two adjacent nodes n and $n+1$ for $n = 1, 2, \dots, N-1$ is assumed to be equal. Here $\eta_{N,M}$ is the efficiency of our parallel and heralded protocol for generating M N -spin GHZ states across N nodes of a quantum network, while $\eta'_{N,M}$ is the corresponding efficiency of protocols that entangle each N spin using one photon.

corresponding efficiency can be described as

$$\eta'_{N,M} = \eta_0^{NM} \eta_d^M \exp[-\alpha M(N-1)L]. \quad (20)$$

Efficiencies $\eta_{N,M}$ and $\eta'_{N,M}$ as a function of the distance L between two adjacent nodes are shown in Fig. 3. Overall, $\eta_{N,M}$ are always larger than $\eta'_{N,M}$ for three different (M, N) . The efficiency enhancement $\eta_{N,M}^{\text{enh}} = \eta_{N,M}(L)/\eta'_{N,M}(L)$ increases notably with L , since we have

$$\eta_{N,M}^{\text{enh}} = \eta_d^{1-M} \exp[\alpha(M-1)(N-1)L]. \quad (21)$$

Specifically, if we take $L = 11$ km, the efficiencies of generating two and five three-qubit entanglements across three nodes by our protocol are $\eta_{3,2}(11) = 0.277$ and $\eta_{3,5}(11) = 0.193$, respectively. However, the corresponding efficiencies described by Eq. (20) are $\eta'_{3,2}(11) = 0.098$ and $\eta'_{3,5}(11) = 3.003 \times 10^{-3}$. For a longer distance $L = 22$ km, our efficiency for generating two and five three-qubit entanglements can reach $\eta_{3,2}(22) = 0.102$ and $\eta_{3,5}(22) = 0.071$, respectively, which are significantly larger than $\eta'_{3,2}(22) = 0.013$ and $\eta'_{3,5}(22) = 2.023 \times 10^{-5}$, which are achieved by protocols entangling each of three spins with one single photon. Moreover, our parallel protocol, for $L > 3.5$ km, can generate five three-qubit entanglement with an efficiency $\eta_{3,5}(L)$ larger than $\eta'_{3,2}(L)$ with which one generates two three-qubit entanglements with two single photons. Moreover, this efficiency enhancement can be further increased for larger (M, N) and longer optical channels, such as $\eta_{4,4}^{\text{enh}}(22) \sim 10^4$ and $\eta_{4,4}^{\text{enh}}(33) \sim 10^6$.

So far, we assume optical switches are perfect with the unity efficiency. In practice, an imperfect optical switch will introduce a photon loss event with a probability $1 - \eta_s$ when a photon passes through it. In our parallel protocol for generating M N -spin GHZ states, we use in total $S_T = (N+1)M - 1$ optical switches to control the transmission of time-bin modes of photon P , when time-bin-dependent delays in the photonics

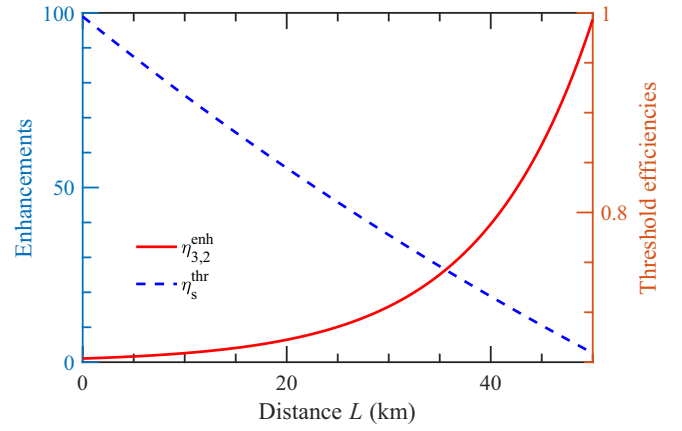


FIG. 4. Enhancements of entanglement generation efficiency and threshold efficiencies of an optical switch for generating in parallel two three-spin GHZ states. The distance L between two adjacent nodes is assumed to be equal. Here $\eta_{3,2}^{\text{enh}}$ is the efficiency enhancement of our protocol for generating two three-spin GHZ states across three nodes, while η_s^{thr} is the threshold efficiency of an optical switch that our protocol can tolerate.

swapping units, i.e., AA , and $AD_{k'}$, are introduced actively in Fig. 2. The efficiency $\eta_{N,M}$ thus should be modified by a factor $\eta_s^{S_T}$, which sets a threshold on the lowest optical switch efficiency η_s^{thr} that depends on M and N in combination with the distance L . The efficiency enhancements $\eta_{3,2}^{\text{enh}}$ and the threshold efficiencies η_s^{thr} as a function of the distance L for $M = 2$ and $N = 3$ are shown in Fig. 4. In general, our parallel protocol can tolerate a lower switch efficiency for a larger L , i.e., $\eta_s^{\text{thr}} = 0.910$ for $L = 11$ km and $\eta_s^{\text{thr}} = 0.831$ for $L = 22$ km, since the efficiency enhancement $\eta_{3,2}^{\text{enh}}$ increases with L for any $M \geq 2$ and $N \geq 3$, shown in Eq. (21). Note that the total number of optical switches for determining the threshold η_s^{thr} is eleven rather than seven, since four additional optical switches in swapping unit AD_2 are used to passively introduce time-bin dependent delays, shown in Fig. 5.

V. DISCUSSION

The essential building block of the parallel and heralded protocol is the effective interface between single photons and individual electron spins of SiV^- in diamond. Recently, such an interface was used to perform asynchronous photonic Bell-state measurement on time-bin encoded photons and then to enhance quantum communication [63]. To implement our protocol for practical multinode quantum networks, the CPF is based on a polarization encoded photon-spin interface, which requires the ability to maintain stability of the phase difference between two paths with different polarizations [65]. In practice, these paths can be combined into one phase-stable architecture by using a monolithic, micron-scale photonic structure with a fidelity larger than 99% [69]. The finite mode matching between the photon polarization and the optical transition polarization of SiV^- leads to an error in the CPF, which decreases its fidelity by 10^{-4} for an achievable mode-matching efficiency of 99% [70].

To effectively modulate the photon states between two adjacent CPFs, the optical switch with an opera-

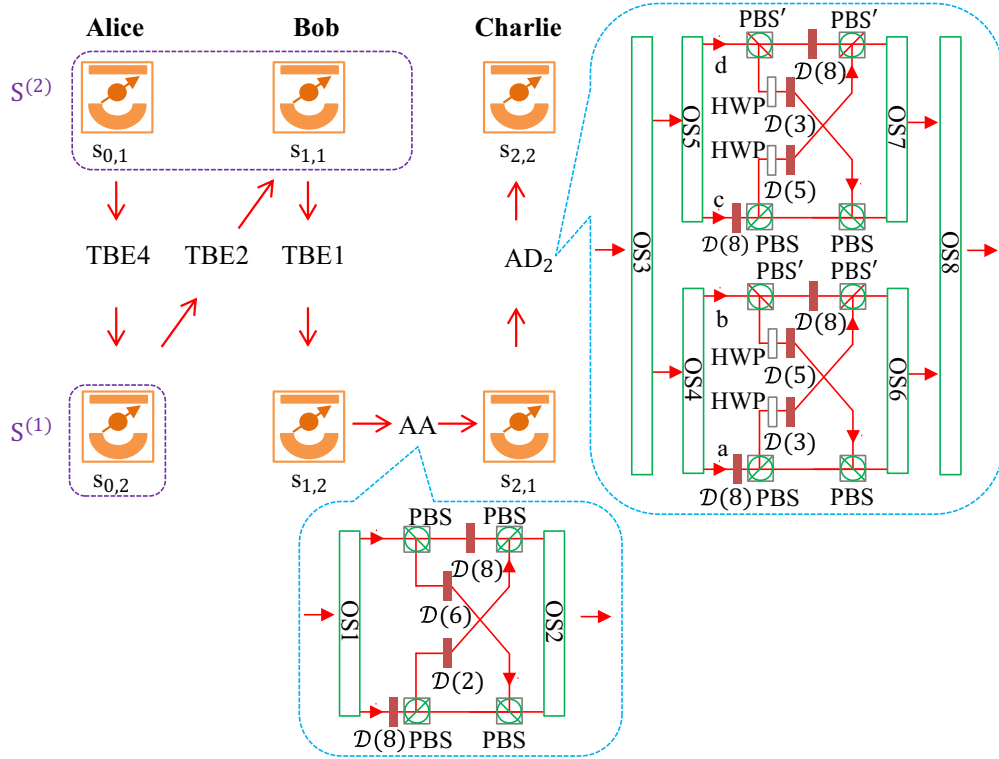


FIG. 5. Schematics of generating two three-spin GHZ states shared by nodes Alice, Bob, and Charlie. Here OS_i ($i = 1, \dots, 8$) is an optical switch and optical elements PBS, PBS', HWP, and $\mathcal{D}(\ast)$ are the same as those used in Fig. 2.

tion time of subnanosecond is needed, which in principle can be constructed by Mach-Zehnder interferometers [70] via electro-optic modulation with subnanosecond phase control [71,72]. Recently, complementary metal-oxide-semiconductor-compatible electro-optic modulators were experimentally demonstrated with data rates up to 210 gigabits/s and an on-chip optical loss of less than 0.5 dB [72].

In general, the decoherence of the SiV^- decreases the fidelity of the nonlocal entanglement generation and its influence on the fidelity can be characterized individually in two different processes: (i) the scattering of the photon in each node and (ii) the propagation of the photon over quantum channels between neighboring nodes. For the former, the decoherence of the electron spin decreases the fidelity of the scattering process by an amount of $\{[1 + \exp(-t_T/T_2^e)]/2\}^M$, when each SiV^- electron spin undergoes individual decoherence [73,74]. Here t_T is the total scattering time in each node, which is in the microsecond range for $M + N \leq 8$ shown in Fig. 3, assuming the time interval $T_\Delta = 1$ ns between two neighboring time bins. The T_2^e is the electron spin coherence time of a SiV^- and exceeds 10 ms at 100 mK [75]. Therefore, the decoherence of the SiV^- electron spin decreases the fidelity of entanglement generation by an amount of less than 0.5% during scattering processes in each node.

To discuss the influence of the decoherence on the fidelity during photon propagation, we make the simplifying assumption that $N - 1$ spins $s_{l,j}$, $l = 0, 1, \dots, N - 2$, are in the same node and spin $s_{N-1,j}$ is in a distant node and that the hybrid entanglement between the first $K + 1$ spins and high-dimensional encoded photon is maximal and ideal, shown in

Eq. (9). The transmission time over a fiber channel of length L' km connecting these nodes is $t_{L'} = L'/c$ (c is the speed of light) and the decoherence of the electron spin will evolve the hybrid maximally entangled state into a mixed entangled state when the photon arrives at the distant node. The probability of state $|\Phi_{K+1}\rangle$ in the mixed entangled state measures the fidelity of entanglement generation of our protocol, when the scattering process in the distance node is ideal and converts hybrid entanglement into multispin entanglement. Therefore, the fidelity of GHZ state generation for each N -spin subsystem is $F = \{[1 + \exp(-t_{L'}/T_2^e)]/2\}^{(N-1)}$ [73,74]. The fidelity $F = 0.95$ can be achieved for $L' = 100$ km, $N = 3$, and $M \leq 5$, which in principle can be increased further by dynamical decoupling or coherent electron-nuclear transfer [75].

VI. CONCLUSION

In summary, we have shown that it is possible to generate in parallel distributed multiqubit entanglement across multiple nodes with a single photon. The influence of exponential loss in optical channels on the entanglement generation can be considerably reduced by using a high-dimensional single photon as a common-data bus. With experimentally accessible parameters, efficiency enhancements of several orders of magnitude can be achieved in some situations. Furthermore, the heralded success of parallel multiqubit entanglement generation is signaled by the detection of a single photon with time-resolved detectors. All these distinguishing features make the parallel and heralded method for multiqubit entanglement generation useful for multinode quantum communication and quantum networks.

ACKNOWLEDGMENTS

This work was supported by the National Natural and Science Foundation of China (Grants No. 11904171, No. 11874212, and No. 11890704), the Program for Innovative Talents and Teams in Jiangsu (Grant No. JSSCTD202138), and the Fundamental Research Funds for the Central Universities (Grant No. 30922010807).

APPENDIX: GENERATING TWO THREE-SPIN GHZ STATES AMONG THREE NODES WITH A SINGLE PHOTON

Here we give a pedagogical example of our protocol for generating two GHZ states among three nodes (Alice, Bob, and Charlie) with the transmission of a single photon, shown in Fig. 5. Here the photon is encoded by an eight-dimensional time-bin mode and a two-dimensional polarization mode; all TBE k_m 's, i.e., $k_m = 2^{(3-m)}$, and swapping units, i.e., AA and AD₂, consist of OSs, $\mathcal{D}(\ast)$, PBSs, PBS's, and HWPs and they can modify the photon state in a similar way as described in Sec. III.

Suppose a SiV⁻ electron spin $s_{l,j}$ ($l = 0, 1, 2$ and $j = 1, 2$) is initialized to the superposition state $|\psi_{s_{l,j}}\rangle = (|g_{s_{l,j}}\rangle + |e_{s_{l,j}}\rangle)/\sqrt{2}$. A D -polarization photon P in Alice's node impinges on the cavity containing $s_{0,1}$ and then passes through the TBE4 circuit, shown in Fig. 2(b) with $\mathcal{D}(k_m) = \mathcal{D}(4)$. Here TBE4 introduces a time delay of $4T_\Delta$ and converts the photon component $|A_0\rangle$ into $|D_4\rangle$. The combined state of photon P and electron spin $s_{0,1}$ evolves into a hybrid entangled state as

$$|\phi_1\rangle = \frac{1}{\sqrt{2}}(|g_{0,1}\rangle|D_0\rangle + |e_{0,1}\rangle|D_4\rangle). \quad (\text{A1})$$

The photon P then interacts with spin $s_{0,2}$ and passes through the TBE2 circuit, which converts all A -polarization components into D -polarization ones with different time bins, i.e., $A_0 \rightarrow D_2$ and $A_4 \rightarrow D_6$. The spins $s_{0,1}, s_{0,2}$ entangle with photon P before it interacts with $s_{1,1}$ in Bob's node as

$$|\phi_2\rangle = \frac{1}{2} \sum_{t=0}^3 \bigotimes_{i=1}^2 \hat{\delta}_{1j_i^{(t)}} |g_{0,1}g_{0,2}\rangle |D_{2t}\rangle. \quad (\text{A2})$$

Here the subscript $t \in \{0, 1, 2, 3\}$ can be translated into a two-bit binary $j_1^{(t)}j_2^{(t)}$ belonging to $\{00, 01, 10, 11\}$; $\hat{\delta}_{1j_i^{(t)}}$ is the identity (bit-flip) operator applied on the i th spin for $j_i^{(t)} = 0$ ($j_i^{(t)} = 1$).

After photon P interacts with $s_{1,1}$ in Bob's node and passes through the TBE1 circuit (it converts $A_{2t} \rightarrow D_{2t+1}$ for $t = 0, 1, 2, 3$), the combined state of three spins $s_{0,1}, s_{0,2}, s_{1,1}$ and photon P evolves into a hybrid entangled state

$$|\phi_3\rangle = \frac{1}{2\sqrt{2}} \sum_{t=0}^7 \bigotimes_{i=1}^3 \hat{\delta}_{1j_i^{(t)}} |g_{0,1}g_{0,2}g_{1,1}\rangle |D_t\rangle, \quad (\text{A3})$$

where the subscript t can be translated into a three-bit binary $j_1^{(t)}j_2^{(t)}j_3^{(t)}$. For instance, when photon P is in state $|D_5\rangle$ with the subscript $t = 5$, we have $j_1^{(t)}j_2^{(t)}j_3^{(t)} = 101$ and $\bigotimes_{i=1}^3 \hat{\delta}_{1j_i^{(t)}} = \hat{\sigma}_1^X \hat{I}_2 \hat{\sigma}_3^X$ and can project three electron spins to state $|e_{0,1}g_{0,2}e_{1,1}\rangle$.

Similarly, we can divide the three electron spins into two parts with $S^{(1)} = s_{0,2}$ and $S^{(2)} = s_{0,1}s_{1,1}$. After the photon interacts with electron spin $s_{1,2}$, a hybrid entangled state is generated between the high-dimensional single photon P and four electron spins, which can be described as

$$|\phi_4\rangle = \frac{1}{4} \sum_{x=0}^7 |G_{S^{(1)}}\rangle_x |G_{S^{(2)}}\rangle_x (|g_{1,2}\rangle|D_x\rangle + |e_{1,2}\rangle|A_x\rangle), \quad (\text{A4})$$

where $|G_{S^{(1)}}\rangle = |g_{0,2}\rangle$, $|G_{S^{(2)}}\rangle = |g_{0,1}g_{1,1}\rangle$, and the subscript x represents the time-bin state of photon P and is exclusively determined by the states of the first three electron spins $s_{0,1}, s_{0,2}, s_{1,1}$, whereas the polarization is determined by electron spin $s_{1,2}$.

The photon P then is transmitted to Charlie and passes through a swapping unit AA consisting of OSs, $\mathcal{D}(\ast)$, and PBSs, as shown in Fig. 5. Here AA swaps the photon components in the A -polarization state with delays $x = j_1^{(1)}j_2^{(1)}j_3^{(1)}$ for those with delays $x_1 = j_1^{(1)}\bar{j}_2^{(1)}j_3^{(1)}$, which can be completed by directing optical time-bin components (0, 1, 4, and 5) [(2, 3, 6, and 7)] to the lower (upper) channel of the swapping unit AA using the OS1. A time delay of $8T_\Delta$ is introduced in both channels to balance the time-bin states of the A -polarization and D -polarization components. Then the OS2 combines all time-bin components into one spatial mode to interact with the electron spin $s_{2,1}$. This swapping unit AA modifies the correlation between the time-bin mode of photon P and the state of $s_{0,1}, s_{0,2}, s_{1,1}$ and completes an effective bit-flip operation on $S^{(1)} = s_{0,2}$ compared with state $|\phi_4\rangle$ when photon P is A polarized. Therefore, after photon P interacts with electron spin $s_{2,1}$, the combined state of $S^{(1)}S^{(2)}s_{1,2}s_{2,1}$ and photon P evolves into

$$|\phi_5\rangle = \frac{1}{4\sqrt{2}} \sum_{x=0}^7 |G_{S^{(2)}}\rangle_x \otimes [(|G_{S^{(1)}}\rangle_x |g_{1,2}g_{2,1}\rangle + |\bar{G}_{S^{(1)}}\rangle_x |e_{1,2}e_{2,1}\rangle)|D_x\rangle + (|G_{S^{(1)}}\rangle_x |g_{1,2}e_{2,1}\rangle + |\bar{G}_{S^{(1)}}\rangle_x |e_{1,2}g_{2,1}\rangle)|A_x\rangle], \quad (\text{A5})$$

where $|\bar{G}_{S^{(1)}}\rangle_x = |G_{S^{(1)}}\rangle_{x_1} = \hat{\sigma}_{s_{0,2}}^X |G_{S^{(1)}}\rangle_x$ and the three electron spins in the last line will be projected into a GHZ state if photon P is measured in the basis $\{|D\rangle, |A\rangle\}$ with time-resolved detectors.

Subsequently, the photon P passes through the swapping unit AD₂, consisting of OSs, $\mathcal{D}(\ast)$, PBSs, PBS's, and HWPs, which exchanges the photon components in the A -polarization state with delays $x = j_1^{(2)}j_2^{(2)}j_3^{(2)}$ and those in D -polarization state with delays $x_2 = \bar{j}_1^{(2)}j_2^{(2)}\bar{j}_3^{(2)}$. This swapping can be achieved by directing time bins (0, 2), (5, 7), (1, 3), and (4, 6) into channels a , b , c , and d of the AD₂ unit, respectively. Therefore, after the photon P passes through the swapping unit AD₂ and interacts with spin $s_{2,2}$, the combined state of the six spins and photon P evolves into

$$|\phi_6\rangle = \frac{1}{4\sqrt{2}} \sum_{x=0}^7 |\varphi_1\rangle_x \otimes [(|G'_{S^{(2)}}\rangle |g_{2,2}\rangle + |\bar{G}'_{S^{(2)}}\rangle |e_{2,2}\rangle)|D_x\rangle + (|G'_{S^{(2)}}\rangle |e_{2,2}\rangle + |\bar{G}'_{S^{(2)}}\rangle |g_{2,2}\rangle)|A_x\rangle], \quad (\text{A6})$$

where $|\varphi_1\rangle_x$ is a GHZ state described by

$$|\varphi_1\rangle_x = \frac{1}{\sqrt{2}}(|G_{S^{(1)}}\rangle_x |G_{1,2}\rangle + |\tilde{G}_{S^{(1)}}\rangle_x |\tilde{G}_{1,2}\rangle), \quad (\text{A7})$$

with

$$|G_{1,2}\rangle = \begin{cases} |g_{1,2}g_{2,1}\rangle, & x < x_2 \\ |g_{1,2}e_{2,1}\rangle, & x > x_2, \end{cases} \quad (\text{A8})$$

and the state of $|G'_{S^{(2)}}\rangle$ can be described by

$$|G'_{S^{(2)}}\rangle = \begin{cases} |G_{S^{(2)}}\rangle_x, & x < x_2 \\ |G_{S^{(2)}}\rangle_{x_2}, & x > x_2 \end{cases} \quad (\text{A9})$$

for $|\tilde{G}_{S^{(2)}}\rangle_x = |G_{S^{(2)}}\rangle_{x_2} = \hat{\sigma}_{s_{0,1}}^x \hat{\sigma}_{s_{1,1}}^x |G_{S^{(2)}}\rangle_x$. Here the electron spins $S^{(1)}_{s_{1,2}g_{2,1}}$ and $S^{(2)}_{s_{2,2}}$ will be simultaneously projected into three-spin GHZ states if photon P is measured in the basis $\{|D\rangle, |A\rangle\}$ with two time-resolved detectors. For instance, if the measurement on photon P reports a result of $|A_5\rangle$, we have $x = 5$, $x_1 = 7$, $x_2 = 0$, $|G_{1,2}\rangle = |g_{1,2}e_{2,1}\rangle$, and $|G'_{S^{(2)}}\rangle = |G_{S^{(2)}}\rangle_0 = |g_{0,1}g_{1,1}\rangle$. The two three-spin subspaces $S^{(1)}_{s_{1,2}g_{2,1}}$ and $S^{(2)}_{s_{2,2}}$ will be projected into state $(|g_{0,2}g_{1,2}e_{2,1}\rangle + |e_{0,2}e_{1,2}g_{2,1}\rangle) \otimes (|g_{0,1}g_{1,1}e_{2,2}\rangle + |e_{0,1}e_{1,1}g_{2,2}\rangle)/2$, which is a product of two nonlocal GHZ states.

-
- [1] D. D. Awschalom, R. Hanson, J. Wrachtrup, and B. B. Zhou, Quantum technologies with optically interfaced solid-state spins, *Nat. Photon.* **12**, 516 (2018).
 - [2] J. Borregaard, A. S. Sørensen, and P. Lodahl, Quantum networks with deterministic spin-photon interfaces, *Adv. Quantum Technol.* **2**, 1800091 (2019).
 - [3] G.-L. Long and X.-S. Liu, Theoretically efficient high-capacity quantum-key-distribution scheme, *Phys. Rev. A* **65**, 032302 (2002).
 - [4] F.-G. Deng, G. L. Long, and X.-S. Liu, Two-step quantum direct communication protocol using the Einstein-Podolsky-Rosen pair block, *Phys. Rev. A* **68**, 042317 (2003).
 - [5] Y. Guo, B.-H. Liu, C.-F. Li, and G.-C. Guo, Advances in quantum dense coding, *Adv. Quantum Technol.* **2**, 1900011 (2019).
 - [6] F. Xu, X. Ma, Q. Zhang, H.-K. Lo, and J.-W. Pan, Secure quantum key distribution with realistic devices, *Rev. Mod. Phys.* **92**, 025002 (2020).
 - [7] Y.-B. Sheng, L. Zhou, and G.-L. Long, One-step quantum secure direct communication, *Sci. Bull.* **67**, 367 (2022).
 - [8] Q. Zhuang, Z. Zhang, and J. H. Shapiro, Distributed quantum sensing using continuous-variable multipartite entanglement, *Phys. Rev. A* **97**, 032329 (2018).
 - [9] P. Yin, Y. Takeuchi, W.-H. Zhang, Z.-Q. Yin, Y. Matsuzaki, X.-X. Peng, X.-Y. Xu, J.-S. Xu, J.-S. Tang, Z.-Q. Zhou, G. Chen, C.-F. Li, and G.-C. Guo, Experimental Demonstration of Secure Quantum Remote Sensing, *Phys. Rev. Appl.* **14**, 014065 (2020).
 - [10] S.-R. Zhao, Y.-Z. Zhang, W.-Z. Liu, J.-Y. Guan, W. Zhang, C.-L. Li, B. Bai, M.-H. Li, Y. Liu, L. You, J. Zhang, J. Fan, F. Xu, Q. Zhang, and J.-W. Pan, Field Demonstration of Distributed Quantum Sensing without Post-Selection, *Phys. Rev. X* **11**, 031009 (2021).
 - [11] Y. L. Lim, A. Beige, and L. C. Kwek, Repeat-Until-Success Linear Optics Distributed Quantum Computing, *Phys. Rev. Lett.* **95**, 030505 (2005).
 - [12] L. Jiang, J. M. Taylor, A. S. Sørensen, and M. D. Lukin, Distributed quantum computation based on small quantum registers, *Phys. Rev. A* **76**, 062323 (2007).
 - [13] W. Qin, X. Wang, A. Miranowicz, Z. Zhong, and F. Nori, Heralded quantum controlled-phase gates with dissipative dynamics in macroscopically distant resonators, *Phys. Rev. A* **96**, 012315 (2017).
 - [14] Y.-B. Sheng and L. Zhou, Distributed secure quantum machine learning, *Sci. Bull.* **62**, 1025 (2017).
 - [15] T. Northup and R. Blatt, Quantum information transfer using photons, *Nat. Photon.* **8**, 356 (2014).
 - [16] D. L. Hurst, K. B. Joanesarson, J. Iles-Smith, J. Mørk, and P. Kok, Generating Maximal Entanglement between Spectrally Distinct Solid-State Emitters, *Phys. Rev. Lett.* **123**, 023603 (2019).
 - [17] C. Wang, Y. Zhang, and G.-S. Jin, Entanglement purification and concentration of electron-spin entangled states using quantum-dot spins in optical microcavities, *Phys. Rev. A* **84**, 032307 (2011).
 - [18] T. Li and F.-G. Deng, Error-rejecting quantum computing with solid-state spins assisted by low- Q optical microcavities, *Phys. Rev. A* **94**, 062310 (2016).
 - [19] S. Mahmoodian, P. Lodahl, and A. S. Sørensen, Quantum Networks with Chiral-Light-Matter Interaction in Waveguides, *Phys. Rev. Lett.* **117**, 240501 (2016).
 - [20] E. Callus and P. Kok, Cumulative generation of maximal entanglement between spectrally distinct qubits using squeezed light, *Phys. Rev. A* **104**, 052407 (2021).
 - [21] C. Y. Hu, A. Young, J. L. O'Brien, W. J. Munro, and J. G. Rarity, Giant optical Faraday rotation induced by a single-electron spin in a quantum dot: Applications to entangling remote spins via a single photon, *Phys. Rev. B* **78**, 085307 (2008).
 - [22] J.-H. An, M. Feng, and C. H. Oh, Quantum-information processing with a single photon by an input-output process with respect to low- Q cavities, *Phys. Rev. A* **79**, 032303 (2009).
 - [23] H.-R. Wei and G. L. Long, Universal photonic quantum gates assisted by ancilla diamond nitrogen-vacancy centers coupled to resonators, *Phys. Rev. A* **91**, 032324 (2015).
 - [24] T. Li, A. Miranowicz, X. Hu, K. Xia, and F. Nori, Quantum memory and gates using a Λ -type quantum emitter coupled to a chiral waveguide, *Phys. Rev. A* **97**, 062318 (2018).
 - [25] S. Daiss, S. Langenfeld, S. Welte, E. Distant, P. Thomas, L. Hartung, O. Morin, and G. Rempe, A quantum-logic gate between distant quantum-network modules, *Science* **371**, 614 (2021).
 - [26] G.-Z. Song, M.-J. Tao, J. Qiu, and H.-R. Wei, Quantum entanglement creation based on quantum scattering in one-dimensional waveguides, *Phys. Rev. A* **106**, 032416 (2022).
 - [27] N. Sangouard, C. Simon, H. de Riedmatten, and N. Gisin, Quantum repeaters based on atomic ensembles and linear optics, *Rev. Mod. Phys.* **83**, 33 (2011).
 - [28] T.-J. Wang, S.-Y. Song, and G. L. Long, Quantum repeater based on spatial entanglement of photons and quantum-dot spins in optical microcavities, *Phys. Rev. A* **85**, 062311 (2012).
 - [29] W. J. Munro, A. M. Stephens, S. J. Devitt, K. A. Harrison, and K. Nemoto, Quantum communication without

- the necessity of quantum memories, *Nat. Photon.* **6**, 777 (2012).
- [30] X.-M. Hu, C.-X. Huang, Y.-B. Sheng, L. Zhou, B.-H. Liu, Y. Guo, C. Zhang, W.-B. Xing, Y.-F. Huang, C.-F. Li, and G.-C. Guo, Long-Distance Entanglement Purification for Quantum Communication, *Phys. Rev. Lett.* **126**, 010503 (2021).
- [31] J. Wu, G.-L. Long, and M. Hayashi, Quantum Secure Direct Communication with Private Dense Coding Using a General Preshared Quantum State, *Phys. Rev. Appl.* **17**, 064011 (2022).
- [32] N. Lo Piparo, W. J. Munro, and K. Nemoto, Quantum multiplexing, *Phys. Rev. A* **99**, 022337 (2019).
- [33] N. Lo Piparo, M. Hanks, C. Gravel, K. Nemoto, and W. J. Munro, Resource Reduction for Distributed Quantum Information Processing Using Quantum Multiplexed Photons, *Phys. Rev. Lett.* **124**, 210503 (2020).
- [34] R. Horodecki, P. Horodecki, M. Horodecki, and K. Horodecki, Quantum entanglement, *Rev. Mod. Phys.* **81**, 865 (2009).
- [35] M. Ardehali, Bell inequalities with a magnitude of violation that grows exponentially with the number of particles, *Phys. Rev. A* **46**, 5375 (1992).
- [36] S. Wehner, D. Elkouss, and R. Hanson, Quantum internet: A vision for the road ahead, *Science* **362**, eaam9288 (2018).
- [37] M. Hillery, V. Bužek, and A. Berthiaume, Quantum secret sharing, *Phys. Rev. A* **59**, 1829 (1999).
- [38] J. Pinnell, I. Nape, M. de Oliveira, N. TabeBordbar, and A. Forbes, Experimental demonstration of 11-dimensional 10-party quantum secret sharing, *Laser Photon. Rev.* **14**, 2000012 (2020).
- [39] T.-J. Wang, G.-Q. Yang, and C. Wang, Control power of high-dimensional controlled teleportation, *Phys. Rev. A* **101**, 012323 (2020).
- [40] L. Pezzè, A. Smerzi, M. K. Oberthaler, R. Schmied, and P. Treutlein, Quantum metrology with nonclassical states of atomic ensembles, *Rev. Mod. Phys.* **90**, 035005 (2018).
- [41] E. Knill, Quantum computing with realistically noisy devices, *Nature (London)* **434**, 39 (2005).
- [42] H.-S. Zhong, Y. Li, W. Li, L.-C. Peng, Z.-E. Su, Y. Hu, Y.-M. He, X. Ding, W. Zhang, H. Li, L. Zhang, Z. Wang, L. You, X.-L. Wang, X. Jiang, L. Li, Y.-A. Chen, N.-L. Liu, C.-Y. Lu, and J.-W. Pan, 12-Photon Entanglement and Scalable Scattershot Boson Sampling with Optimal Entangled-Photon Pairs from Parametric Down-Conversion, *Phys. Rev. Lett.* **121**, 250505 (2018).
- [43] Y. Zhou, B. Li, X.-X. Li, F.-L. Li, and P.-B. Li, Preparing multiparticle entangled states of nitrogen-vacancy centers via adiabatic ground-state transitions, *Phys. Rev. A* **98**, 052346 (2018).
- [44] Y.-F. Qiao, H.-Z. Li, X.-L. Dong, J.-Q. Chen, Y. Zhou, and P.-B. Li, Phononic-waveguide-assisted steady-state entanglement of silicon-vacancy centers, *Phys. Rev. A* **101**, 042313 (2020).
- [45] W. Qin, A. Miranowicz, H. Jing, and F. Nori, Generating Long-Lived Macroscopically Distinct Superposition States in Atomic Ensembles, *Phys. Rev. Lett.* **127**, 093602 (2021).
- [46] A. Reiserer, N. Kalb, G. Rempe, and S. Ritter, A quantum gate between a flying optical photon and a single trapped atom, *Nature (London)* **508**, 237 (2014).
- [47] C. T. Nguyen, D. D. Sukachev, M. K. Bhaskar, B. Machielse, D. S. Levonian, E. N. Knall, P. Stroganov, R. Riedinger, H. Park, M. Lončar, and M. D. Lukin, Quantum Network Nodes Based on Diamond Qubits with an Efficient Nanophotonic Interface, *Phys. Rev. Lett.* **123**, 183602 (2019).
- [48] T. Li, G.-J. Yang, and F.-G. Deng, Heralded quantum repeater for a quantum communication network based on quantum dots embedded in optical microcavities, *Phys. Rev. A* **93**, 012302 (2016).
- [49] M. Zukowski, A. Zeilinger, and H. Weinfurter, Entangling photons radiated by independent pulsed sources, *Ann. N.Y. Acad. Sci.* **755**, 91 (1995).
- [50] S. Bose, V. Vedral, and P. L. Knight, Multiparticle generalization of entanglement swapping, *Phys. Rev. A* **57**, 822 (1998).
- [51] C.-Y. Lu, T. Yang, and J.-W. Pan, Experimental Multiparticle Entanglement Swapping for Quantum Networking, *Phys. Rev. Lett.* **103**, 020501 (2009).
- [52] T. Li, A. Miranowicz, K. Xia, and F. Nori, Resource-efficient analyzer of Bell and Greenberger-Horne-Zeilinger states of multiphoton systems, *Phys. Rev. A* **100**, 052302 (2019).
- [53] I. Buluta, S. Ashhab, and F. Nori, Natural and artificial atoms for quantum computation, *Rep. Prog. Phys.* **74**, 104401 (2011).
- [54] Y. Zhong, H.-S. Chang, A. Bienfait, E. Dumur, M.-H. Chou, C. R. Conner, J. Grebel, R. G. Povey, H. Yan, D. I. Schuster, and A. N. Cleland, Deterministic multi-qubit entanglement in a quantum network, *Nature (London)* **590**, 571 (2021).
- [55] M. Pompili, S. L. N. Hermans, S. Baier, H. K. C. Beukers, P. C. Humphreys, R. N. Schouten, R. F. L. Vermeulen, M. J. Tiggeleman, L. dos Santos Martins, B. Dirkse, S. Wehner, and R. Hanson, Realization of a multinode quantum network of remote solid-state qubits, *Science* **372**, 259 (2021).
- [56] A. Cervera-Lierta, M. Krenn, A. Aspuru-Guzik, and A. Galda, Experimental High-Dimensional Greenberger-Horne-Zeilinger Entanglement with Superconducting Transmon Qutrits, *Phys. Rev. Appl.* **17**, 024062 (2022).
- [57] S. Perseguers, G. Lapeyre, Jr., D. Cavalcanti, M. Lewenstein, and A. Acín, Distribution of entanglement in large-scale quantum networks, *Rep. Prog. Phys.* **76**, 096001 (2013).
- [58] D.-Y. Cao, B.-H. Liu, Z. Wang, Y.-F. Huang, C.-F. Li, and G.-C. Guo, Multiuser-to-multiuser entanglement distribution based on 1550 nm polarization-entangled photons, *Sci. Bull.* **60**, 1128 (2015).
- [59] W. Qin and F. Nori, Controllable single-photon transport between remote coupled-cavity arrays, *Phys. Rev. A* **93**, 032337 (2016).
- [60] R. Uppu, L. Midolo, X. Zhou, J. Carolan, and P. Lodahl, Quantum-dot-based deterministic photon-emitter interfaces for scalable photonic quantum technology, *Nat. Nanotechnol.* **16**, 1308 (2021).
- [61] M. Ruf, N. H. Wan, H. Choi, D. Englund, and R. Hanson, Quantum networks based on color centers in diamond, *J. Appl. Phys.* **130**, 070901 (2021).
- [62] C. T. Nguyen, D. D. Sukachev, M. K. Bhaskar, B. Machielse, D. S. Levonian, E. N. Knall, P. Stroganov, C. Chia, M. J. Burek, R. Riedinger, H. Park, M. Lončar, and M. D. Lukin, An integrated nanophotonic quantum register based on silicon-vacancy spins in diamond, *Phys. Rev. B* **100**, 165428 (2019).
- [63] M. K. Bhaskar, R. Riedinger, B. Machielse, D. S. Levonian, C. T. Nguyen, E. N. Knall, H. Park, D. Englund, M. Lončar, D. D. Sukachev, and M. D. Lukin, Experimental demonstration of memory-enhanced quantum communication, *Nature (London)* **580**, 60 (2020).

- [64] M. Erhard, M. Krenn, and A. Zeilinger, Advances in high-dimensional quantum entanglement, *Nat. Rev. Phys.* **2**, 365 (2020).
- [65] A. Reiserer and G. Rempe, Cavity-based quantum networks with single atoms and optical photons, *Rev. Mod. Phys.* **87**, 1379 (2015).
- [66] B. Hensen, H. Bernien, A. E. Dréau, A. Reiserer, N. Kalb, M. S. Blok, J. Ruitenberg, R. F. Vermeulen, R. N. Schouten, C. Abellán, W. Amaya, V. Pruneri, M. W. Mitchell, M. Markham, D. J. Twitchen, D. Elkouss, S. Wehner, T. H. Taminiau, and R. Hanson, Loophole-free Bell inequality violation using electron spins separated by 1.3 kilometres, *Nature (London)* **526**, 682 (2015).
- [67] S. Meesala, Y.-I. Sohn, B. Pingault, L. Shao, H. A. Atikian, J. Holzgrafe, M. Gündoğan, C. Stavrakas, A. Sipahigil, C. Chia, R. Evans, M. J. Burek, M. Zhang, L. Wu, J. L. Pacheco, J. Abraham, E. Bielejec, M. D. Lukin, M. Atatüre, and M. Lončar, Strain engineering of the silicon-vacancy center in diamond, *Phys. Rev. B* **97**, 205444 (2018).
- [68] B. Machielse, S. Bogdanovic, S. Meesala, S. Gauthier, M. J. Burek, G. Joe, M. Chalupnik, Y. I. Sohn, J. Holzgrafe, R. E. Evans, C. Chia, H. Atikian, M. K. Bhaskar, D. D. Sukachev, L. Shao, S. Maity, M. D. Lukin, and M. Lončar, Quantum Interference of Electromechanically Stabilized Emitters in Nanophotonic Devices, *Phys. Rev. X* **9**, 031022 (2019).
- [69] K. C. Chen, E. Bersin, and D. Englund, A polarization encoded photon-to-spin interface, *npj Quantum Inf.* **7**, 2 (2021).
- [70] J. Borregaard, H. Pichler, T. Schröder, M. D. Lukin, P. Lodahl, and A. S. Sørensen, One-Way Quantum Repeater Based on Near-Deterministic Photon-Emitter Interfaces, *Phys. Rev. X* **10**, 021071 (2020).
- [71] G. T. Reed, G. Mashanovich, F. Y. Gardes, and D. J. Thomson, Silicon optical modulators, *Nat. Photon.* **4**, 518 (2010).
- [72] C. Wang, M. Zhang, X. Chen, M. Bertrand, A. Shams-Ansari, S. Chandrasekhar, P. Winzer, and M. Lončar, Integrated lithium niobate electro-optic modulators operating at CMOS-compatible voltages, *Nature (London)* **562**, 101 (2018).
- [73] W. Dür and H.-J. Briegel, Stability of Macroscopic Entanglement under Decoherence, *Phys. Rev. Lett.* **92**, 180403 (2004).
- [74] L. Aolita, D. Cavalcanti, A. Acín, A. Salles, M. Tiersch, A. Buchleitner, and F. de Melo, Scalability of Greenberger-Horne-Zeilinger and random-state entanglement in the presence of decoherence, *Phys. Rev. A* **79**, 032322 (2009).
- [75] D. D. Sukachev, A. Sipahigil, C. T. Nguyen, M. K. Bhaskar, R. E. Evans, F. Jelezko, and M. D. Lukin, Silicon-Vacancy Spin Qubit in Diamond: A Quantum Memory Exceeding 10 ms with Single-Shot State Readout, *Phys. Rev. Lett.* **119**, 223602 (2017).